Water and Soil Management and Modeling

Online ISSN: 2783 - 2546

University of Mohaghegh Ardabili

Analysis of hydrodynamic patterns in the coastal waters of the Caspian Sea using field measurements

Abbas Einali [1*], Mohammad Akbari Nasab [2], Mohammad Hossein Nemati [3]

[1*] Assistant professor, Faculty of Environmental and Marine Sciences, University of Mazandaran, Mazandaran, Iran.
[2] Associate professor of Physical Oceanography, Faculty of Environmental and Marine Sciences, University of Mazandaran, Mazandaran, Iran.
[3] MSc. in Physical Oceanography, Port and Maritime Organization, Tehran, Iran.

Abstract

This study investigates the wave and current dynamics of the Caspian Sea, the world's largest enclosed inland water body, with a focus on its southern coast. The Caspian's meridional axis, diverse climatic conditions, and complex coastal morphology contribute to highly variable hydrodynamic behavior, yet oceanographic data in the region remain scarce. To address this gap, wave and current measurements were conducted for about 14 months at seven nearshore stations—five at 10 meters and two at 30 meters depth—spanning east to west along Iran's coastline. Data were collected using Acoustic Doppler Current Profilers (ADCP), including AWAC and AquaDopp systems, configured for high-resolution profiling of surface and bottom layers. All measurements underwent multi-layered quality control using PMODynamics software, and descriptive statistical indicators such as mean, maximum, variance, and standard deviation were calculated to assess seasonal and spatial variability. The results confirmed the Caspian Sea's counterclockwise circulation, with eastward currents prevailing in central and eastern stations (Noshahr, Anzali, Amirabad), and southward flows dominating western stations (Astara). Roudsar showed localized eddy activity, reversing the dominant flow. Seasonal analysis revealed that winter produced the most intense hydrodynamic conditions, with surface current speeds reaching up to 1.15 m/s at Amirabad and standard deviations peaking at 0.16 m/s in autumn. Bottom currents remained more stable, with mean speeds below 0.13 m/s and minimal variance. Wave conditions also varied significantly across stations and seasons. Anzali recorded the most intense wave regime, with significant wave heights frequently ranging between 0.8 and 1.2 meters, especially during autumn and winter. In contrast, spring exhibited the lowest variability, with standard deviations under 0.35 meters at most stations. These patterns reflect the influence of seasonal wind forcing and coastal morphology on wave behavior. These findings provide essential baseline data for coastal management, sediment transport modeling, and infrastructure design in a region increasingly affected by climate change and water level fluctuations.

Keywords: Caspian Sea, Acoustic Doppler Current Profiler (ADCP), coastal currents, wave height variability, seasonal hydrodynamics.

Article Type: Research Article
Academic Editor: Raoof Mostafazadeh

[*]Corresponding Author, E-mail: a.einali84@umz.ac.ir
Citation: Einali, A., Akbari Nasab, M., & Nemati, M. H. (2026). Analysis of hydrodynamic patterns in the coastal waters of the Caspian Sea using field measurements. Water and Soil Management and Modeling, 6(2) (Special Issue: New Approaches to Water and Soil Management and Modeling), 89-120.
doi: 10.22098/mmws.2025.18495.1698
Received: 05 October 2025, Received in revised form: 11 November 2025, Accepted: 11 November 2025, Published online: 03 June 2026
Water and Soil Management and Modeling, Year 2026, Vol. 6, No.2 (Special Issue), pp. 89-120
Publisher: University of Mohaghegh Ardabili

1. Introduction

The Caspian Sea, the largest enclosed inland body of water on Earth, is bordered by five countries: Russia, Kazakhstan, Turkmenistan, Iran, and Azerbaijan. It has a unique geographical setting with a surface area of approximately 371,000 square kilometers and a maximum depth of about 1,025 meters (Chicherina et al., 2004; Mamaev, 2002). The climate around the Caspian Sea varies significantly, with the northern part experiencing cold winters and hot summers, while the southern part has milder winters and hotter summers. The general wind patterns and atmospheric systems affecting the Caspian Sea include the Siberian High, which brings cold air masses, and the Azores High, which influences the summer weather (Nejat et al., 2018). The overall water circulation in the Caspian Sea is cyclonic, and wave conditions are influenced by wind patterns and the basin's morphology (Azizpour & Ghaffari, 2023).

The southern coast of the Caspian Sea is characterized by diverse bathymetric features, with depths ranging from shallow coastal areas to deeper offshore regions. The coastal morphology is influenced by sediment deposition and erosion processes, which are driven by wave and current dynamics (Alemi Safaval et al., 2018; Firoozfar et al., 2014). The general circulation of water in the southern Caspian Sea is influenced by wind-driven currents and the basin's topography, leading to complex flow patterns. Wave conditions in this region are primarily affected by local wind patterns and can vary significantly depending on seasonal changes (Ghaffari & Chegini, 2010).

Field measurements of wave and current parameters are crucial in oceanographic studies as they provide essential data for understanding the physical dynamics of marine environments. These measurements help assess the impact of climatic changes on ocean circulation, wave patterns, and coastal erosion (Bellafiore et al., 2011; Thomas & Cheung, 2024). Accurate field data are necessary for validating numerical models and improving the predictability of oceanographic phenomena, which is vital for coastal management and marine resource exploitation (Gould et al., 2013; Williams, 2011). Despite its significance, the Caspian Sea lacks comprehensive oceanographic data, particularly regarding wave and current measurements. This scarcity of data hampers the ability to fully understand the sea's dynamic processes and their implications for the surrounding environment (Ghaffari & Chegini, 2010). The limited availability of observational data is a significant challenge for researchers, making it difficult to develop accurate models and forecasts for the region (Azizpour & Ghaffari, 2023; Nejat et al., 2018).

Longshore Currents demonstrate the interaction of air, land, and sea. Currents are directly related to the wind and also through waves. On the other hand, currents affect sediment transport and coastal morphology. The topographic structure and coastal morphology also affect coastal currents (Dodet et al., 2019; Johansson et al., 2022; Melet et al., 2020). Accordingly, the counterclockwise circulation of the Caspian Sea water has an important impact on hydrodynamics, hydrophysics, and coastal morphology (Lavrova et al., 2011).

Recent studies have utilized Acoustic Doppler Current Profilers (ADCP) to measure wave and current parameters in the Caspian Sea. In 2010, Ghaffari and Chegini conducted a study titled "Acoustic Doppler Current Profiler Observations in the Southern Caspian Sea: Shelf Currents and Flow Field off Feridoonkenar Bay, Iran." This research involved offshore bottom-mounted ADCP measurements and wind records to characterize current fields in the continental shelf and offshore deeper regions in the southern Caspian Sea. The results indicated that long-period waves dominate the current field in the continental shelf off Feridoonkenar Bay. The study found that the prevailing wind patterns significantly influence the current profiles observed during the measurements (Ghaffari & Chegini, 2010). In 2014, Firoozfar and Neshaei researched sediment deposition and erosion processes along the southern coast, showing that local wave patterns significantly impact coastal morphology (Firoozfar et al., 2014). In 2024, Zavialov and Kostianoy conducted a study on the Kazakhstan shelf of the Caspian Sea, revealing that the currents were predominantly along the shore but simultaneously variable in direction.

The results also indicated that the along-shore wind stress significantly influenced the wave and current dynamics (Zavialov et al., 2024). In 2019, Masoud et al. conducted a study titled "Low-Frequency Variations in Currents on the Southern Continental Shelf of the Caspian Sea." This research evaluated wind-induced currents along the southern Caspian Sea, revealing that low-frequency variations in currents were significantly influenced by wind patterns (Masoud et al., 2019).

Today, the use of acoustic current meters and wave meters is considered the best method for measuring wave and current parameters in the marine environment. The reason for this is the possibility of recording minor and instantaneous changes due to high accuracy and recording vertical and horizontal profiles with the desired accuracy of waves and currents in the marine environment. The absence of mechanical parts in this type of device is another important advantage of these devices. It reduces the possibility of their failure and provides the ability to use the device for a long time at sea (Williams, 1996).

Although previous studies have employed ADCP and other acoustic instruments in parts of the Caspian Sea, multi-seasonal field measurements across several nearshore stations—especially with simultaneous surface and bottom layer profiling—have rarely been conducted. The limited availability of such high-resolution datasets has constrained the ability to analyze spatial-temporal hydrodynamic variability in this region. This study aims to address that gap by providing validated measurements over a full annual cycle, supporting improved understanding of coastal circulation patterns and their implications for sediment transport and shoreline management.

In this study, considering the importance of field measurements in oceanography and the lack of this type of information in the Caspian Sea, using acoustic wave and current measurement devices (ADCP), wave and current information was recorded at seven nearshore stations (five 10-meter stations and two 30-meter stations) on the southern coast of the Caspian Sea in Iran over more than a year. This information was recorded in different water column layers, which in this study considered surface and bottom layer information. Then, the recorded information was analyzed and examined temporarily and spatially. For this purpose, various diagrams were used, including wind rose, wave rose, scatter diagram, and radar diagram.

2. Materials and Methods

The study area encompasses the southern coasts of the Caspian Sea in Iran, extending from the westernmost point at Astara Port to Amirabad Port in the east. The sampling stations are located within the areas of the ports, including Astara, Anzali, Noshahr, Roudsar, and Amirabad. At all ports, one station with a depth of 10 meters was selected, while at Astara and Roudsar, an additional station with a depth of 30 meters was also considered. Data collection was conducted from December 2012 to January 2014. The measured parameters included current characteristics, such as velocity and direction across different layers, and wave parameters, including significant wave height and direction. Figure 1 shows the location of the Caspian Sea and the study area (southern shores of the Caspian Sea). Using acoustic waves and the Doppler effect has transformed how ocean currents and wave parameters are measured. Acoustic Doppler systems transmit sound waves into the water, which are reflected by suspended particles and scatterers. The frequency shift in the returned signals, caused by the relative motion of these particles, is analyzed to calculate current velocities with high accuracy. This method enables comprehensive three-dimensional profiling of water column movements and provides critical insights into wave orbital velocities. The ability to gather precise hydrodynamic data has made this approach invaluable for understanding complex marine processes and supporting various applications, including coastal engineering and environmental monitoring (Birch et al., 2004; Rao et al., 2017).

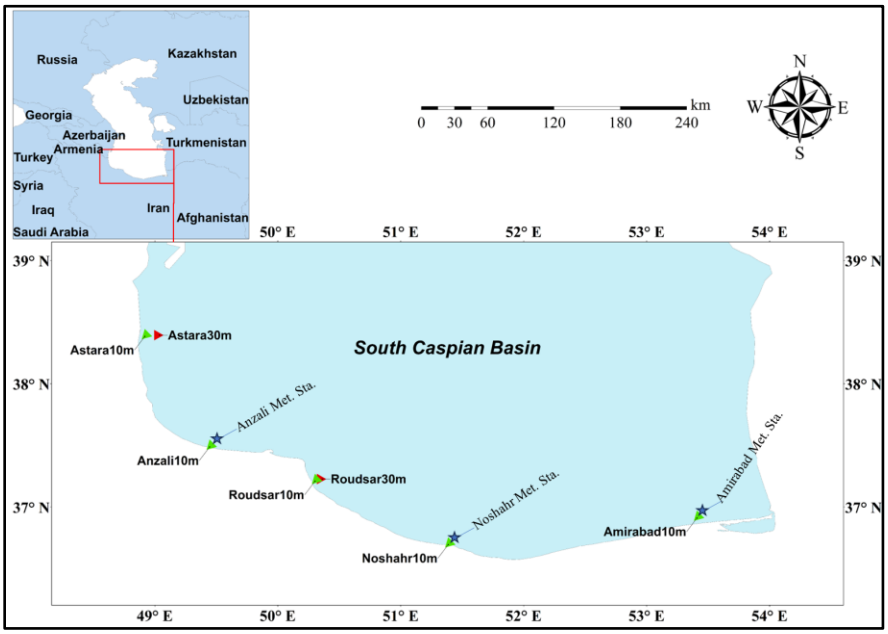

Figure. 1. Geographical location of the Caspian Sea and the study area along its southern coastline. The map shows ADCP-based current and wave measurement stations (triangles) and coastal meteorological stations (Stars) used for wind data collection.

The Acoustic Wave and Current (AWAC) profiler, developed by Nortek, stands out as a robust instrument that integrates current profiling and wave measurement. The AWAC utilizes three-dimensional current profiling technology alongside a vertically aligned acoustic beam for surface tracking, ensuring accurate wave height, period, and direction measurement. This dual functionality allows for simultaneous data collection, streamlining the process and eliminating the need for multiple devices. With its reliable performance and precise data acquisition, the AWAC is ideal for applications ranging from coastal hydrodynamics studies to offshore engineering (Nortek, 2025b)

Similarly, the AquaDopp, another advanced profiler by Nortek, is designed to accurately measure ocean currents in diverse environments. By transmitting sound waves and analyzing frequency shifts caused by the Doppler effect, the AquaDopp determines current velocities across multiple depth layers. Its versatility lies in its ability to function effectively in shallow and deep waters. The AquaDopp is highly adaptable to challenging marine conditions with a compact design and durable construction. It is a valuable tool for three-dimensional current profiling, supporting studies in sediment transport, coastal monitoring, and oceanographic research (Nortek, 2025a).

At the Anzali station, the AquaDopp profiler was deployed with specific settings tailored to the study's objectives. Wave data were collected hourly over 1024 seconds at a sampling frequency of 2 Hz, ensuring high-resolution wave parameter measurements. Additionally, current profiles, including velocity and direction, were recorded every 10 minutes at vertical intervals of 0.5 meters and averaged over 90 seconds to provide detailed insights into currents' temporal and spatial variability. In contrast, the Acoustic Wave and Current (AWAC) profiler was used at the other stations, and the configurations were optimized for comprehensive data collection. Wave data were recorded hourly with 2400 samples at a 2 Hz frequency, allowing for precise wave measurements. Current profiling was conducted at the same 10-minute intervals with 0.5-meter depth resolution, but the data were averaged over 150 seconds. These tailored setups ensured reliable and consistent data collection across all stations, enabling a robust analysis of hydrodynamic conditions.

In parallel with wave and current measurements, meteorological data—including wind speed and direction—were also recorded at three coastal

stations: Anzali, Noshahr, and Amirabad. These wind observations were synchronized with the ADCP deployments and collected over the same temporal intervals to ensure consistency across datasets. Although detailed wind analysis is beyond the scope of this study, the wind data serve as complementary inputs for interpreting hydrodynamic variability.

The selection of measurement stations in this study was based on a combination of scientific, operational, and engineering considerations. Stations were strategically distributed along the southern coast of the Caspian Sea to ensure adequate spatial coverage from east to west. Their proximity to active ports facilitated logistical support and safe deployment and retrieval of equipment, while also enabling the application of collected data in port development projects, optimization of coastal structures, and engineering designs based on real wave and current conditions. Although the study focused geographically on Iran's southern coasts, the general circulation of Caspian Sea waters was also considered in the interpretation of results.

Given the importance of data reliability in oceanographic studies, all wave and current measurements used in this research were subjected to a comprehensive quality control process prior to analysis. This process was performed automatically using the quality control plugin embedded in the PMODynamics software. Within the software, the Caspian Sea was selected as the target region, allowing the plugin to apply region-specific and global thresholds to evaluate the data accordingly (PMDynamics_Team, 2018) At this stage, invalid data were excluded, ensuring that only reliable measurements were used in the regional analysis. The quality control tests implemented by the PMODynamics plugin are categorized into two main groups: general tests and specific tests. General tests are designed to identify missing, outlier, or unrealistic values across spatial and temporal series. These include the Gap Test for detecting missing records, the Range Test to verify that values fall within acceptable physical limits (e.g., current speeds typically range between 0 and 1 m/s in the southern Caspian Sea), the Maximum Gradient Test to assess abrupt changes between consecutive observations using $| x_i - x_{i-1} | <$ Threshold , where x_i is the current value, x_{i-1} is the previous value, and Threshold is the maximum allowed change. The Data Freeze Test identifies values that remain unchanged for an unusually long duration, and the Spike Test detects sudden deviations from neighboring values using Spike $= x_2 - (x_1 + x_3/2)$, where x_2 is the value under evaluation, and x_1, x_3 are its adjacent values.

Specific tests focus on physical and regional consistency. These include the Regional Validity Test, which compares data against acceptable thresholds for the Caspian Sea.

The Vertical Gradient Test for Currents evaluates current velocity changes across depth layers using $| V_m - (V_{m-1} + V_{m+1}/2) | < \Delta V$, where V_m is the current velocity at depth m, V_{m-1} and V_{m+1} are velocities at adjacent depths, and ΔV is the threshold. Additionally, the Wave Height–Period Relationship Test ensures that wave height H_s and wave period T_p follow the expected empirical relationship as $H_s \propto T_p^2$. Values that deviate significantly from this pattern are flagged as suspicious or discarded.

To complete the validation process, statistical tests were also applied. The Standard Deviation Test assessed data dispersion relative to the mean $\sigma = (1/N \sum_{i=1}^{N} (x_i - \mu)^2)^{1/2}$, where x_i is each data point, μ is the mean, N is the number of observations, and σ is the standard deviation. Data points exceeding two standard deviations from the mean were removed. The Confidence Interval Test defined the range of acceptable values at a 95% confidence level as $\mu \pm 1.96 \cdot \frac{\sigma}{\sqrt{N}}$, where μ is the mean, σ is the standard deviation, and N is the sample size. Values outside this interval were considered unreliable (PMDynamics_Team, 2018).

This multi-layered quality control ensured that all data used in the study were scientifically valid and regionally appropriate.

As a direct outcome of the multi-layered quality control procedures described above, a visual matrix was constructed to summarize the temporal validity of the dataset across all measurement stations and calendar months. In this matrix, each row corresponds to a specific station and each column represents a month. The color coding reflects the results of automated

validation: green cells indicate periods where data passed all quality control checks and were considered reliable, while red cells denote time intervals with missing, incomplete, or invalid data that were excluded from further analysis. Table 1 provides a concise overview of data integrity across both spatial and temporal dimensions, helping to identify seasonal gaps, station-specific inconsistencies, and overall coverage quality prior to interpretation and modeling.

Table 1. Monthly data validity matrix for all measurement stations based on automated quality control results.

	2012		2013												2014	
	November	December	January	February	March	April	May	June	July	August	September	October	November	December	January	February
Astara 30m	-	***	**********	*	**********	**********	**********	**********	**********	**********	**********	**********	**********	**********	****-	-
Astara 10m	-	***	**********	*	**********	**********	**********	**********	**********	**********	**********	**********	**********	**********	****-	-
Anzali 10m	-	*****	*******		*******	**********	**********	**********	**********	**********	**********	**********	**********	**********	*---	-
Roudsar 10m	*	**********	**********	*	**********	**********	**********	**********	**********	**********	**********	**********	**********	**********	*---	-
Roudsar 30m	-	**********	**********	*	**********	**********	**********	**********	**********	**********	**********	*********	**********	**********	******	-
Noshahr 10m	-	****	**********	*	**********	**********	**********	**********	**********	**********	**********	**********	**********	**********	**********	*
Amirabad 10m	*	****	**********	*	**********	**********	**********	**********	**********	**********	**********	**********	**********	**********	******	-

Note: *= Valid data, NA = Invalid data, - = an explanation

3. Results

This section presents the results of more than a year of measuring wave and current parameters at seven stations on the southern coast of the Caspian Sea using ADCP devices, the most accurate measuring equipment in this field. To better understand the wave and current conditions, a variety of diagrams such as wave rose, current rose, Seasonal radar chart of wave and current, wave and current probability, direction and speed distribution, and direction-speed scatter plots have been used; a few of which are presented in this article, but all of them have been used to analyze the results.

3-1. Currents

This section presents the descriptive statistical indicators of marine currents at seven coastal stations over four seasons, with separate analyses for surface and bottom layers. The statistical parameters include maximum, minimum, mean, variance, and standard deviation, providing insight into both the magnitude and variability of current behavior across time and space.

The surface currents exhibited broader variability compared to bottom flows. In winter, maximum surface current speeds reached up to 1.15 m/s at certain stations, while standard deviations in autumn peaked at 0.16 m/s. These elevated values reflect substantial dispersion in the dataset, indicating the presence of highly dynamic current regimes. Such fluctuations are likely driven by wind forcing, surface pressure gradients, and seasonal instability in the upper water column. Mean surface current speeds ranged from 0.10 to 0.24 m/s across seasons, with variance values between 0.01 and 0.02, confirming the energetic nature of surface circulation, particularly during autumn and winter.

In contrast, bottom currents showed more stable behavior. Maximum speeds rarely exceeded 0.79 m/s, and standard deviations remained below 0.11 m/s in most cases. Mean values were generally lower, ranging from 0.08 to 0.13 m/s, and variance values were consistently minimal (mostly below 0.01). These patterns suggest that bottom-layer flows are less susceptible to short-term fluctuations and may be governed more by bathymetric constraints and residual circulation than by surface forcing.

Comparative analysis of variance and standard deviation across both layers reveals that surface currents are generally more variable and energetic than bottom flows. This contrast is most pronounced during autumn and winter, when surface layer instability intensifies. These

findings have important implications for sediment transport, vertical mixing, and the design of coastal and subaqueous infrastructure.

A detailed summary of the descriptive statistics for surface and bottom currents is presented in Table 2 and Table 3.

To statistically evaluate the relationship between marine currents and wave conditions, Pearson correlation coefficients were calculated based on seasonal mean values of significant wave height and current velocity in both surface and bottom layers across all stations. The results indicated that the correlations were notably stronger during autumn and winter, with r values of 0.72 and 0.60 for surface currents, and 0.53 and 0.57 for bottom currents, respectively. These positive correlations suggest that during more energetic periods of the year—such as autumn and winter—surface and bottom currents tend to interact more closely with wave dynamics, likely due to intensified wind forcing and enhanced vertical mixing within the water column. In contrast, spring and summer exhibited weak or negative correlations, implying that under calmer conditions, wave and current behavior may be governed by distinct mechanisms. The seasonal alignment between elevated correlation values and the recorded maxima in wave height and current speed reinforces the role of dynamic coupling in shaping coastal hydrodynamic patterns during unstable periods.

Table 2. Descriptive statistics of surface currents at seven coastal stations over four seasons

		Roudsar 30m	Roudsar 10m	Astara 10m	Astara 30m	Anzali 10m	Noshahr 10m	Amirabad 10m
Winter	Max	0.42	0.79	0.85	0.59	0.70	0.82	1.15
	Min	0.00	0.00	0.00	0.00	0.00	0.00	0.00
	Average	0.42	0.12	0.14	0.11	0.16	0.14	0.11
	Variance	0.00	0.01	0.01	0.01	0.02	0.01	0.01
	SD	0.06	0.08	0.12	0.10	0.13	0.10	0.09
Spring	Max	0.64	0.51	0.88	0.46	0.41	0.63	0.50
	Min	0.00	0.00	0.00	0.00	0.00	0.00	0.00
	Average	0.15	0.14	0.13	0.15	0.12	0.15	0.10
	Variance	0.01	0.01	0.01	0.01	0.01	0.01	0.00
	SD	0.10	0.09	0.09	0.09	0.08	0.10	0.06
Summer	Max	0.54	0.50	0.59	0.57	0.47	0.52	0.43
	Min	0.00	0.00	0.00	0.00	0.00	0.00	0.00
	Average	0.16	0.12	0.12	0.19	0.14	0.15	0.12
	Variance	0.01	0.01	0.01	0.01	0.01	0.01	0.01
	SD	0.10	0.08	0.08	0.11	0.08	0.08	0.08
Autumn	Max	0.71	0.80	0.85	0.90	0.82	0.92	0.68
	Min	0.00	0.00	0.00	0.00	0.00	0.00	0.00
	Average	0.17	0.13	0.16	0.24	0.19	0.18	0.11
	Variance	0.01	0.01	0.02	0.02	0.02	0.02	0.01
	SD	0.12	0.09	0.13	0.16	0.15	0.15	0.10

The preceding statistical analysis provides a quantitative overview of current magnitudes and variability across stations and seasons. In the following sections, we examine the spatial and temporal patterns of current directions to better understand regional hydrodynamic behavior.

The general pattern of current directions along the southern coast of the Caspian Sea reveals a consistent eastward tendency in central and eastern stations. At Noshahr, Anzali, and Amirabad (all 10 m depth), the prevailing current direction at both surface and bottom layers is dominantly eastward (E, ENE, ESE), with

opposing westward currents (W, WSW) appearing less frequently and with lower energy. For instance, at Noshahr, the surface currents are primarily channeled between E and W, while bottom currents show broader directional dispersion. Similarly, at Anzali, eastward currents significantly outpace westward ones, and over 60% of bottom currents fall within the 0–0.1 m/s speed range. At Amirabad, ENE currents dominate both layers, with more than half of the currents at each depth exhibiting speeds below 0.1 m/s. These observations suggest a stable hydrodynamic regime in the central and eastern stations, shaped by regional wind forcing and basin-scale circulation.

Table 3. Descriptive statistics of bottom currents at seven coastal stations over four seasons

		Roudsar 30m	Roudsar 10m	Astara 10m	Astara 30m	Anzali 10m	Noshahr 10m	Amirabad 10m
Winter	Max	0.29	0.38	0.45	0.49	0.52	0.65	0.63
	Min	0.00	0.00	0.00	0.00	0.00	0.00	0.00
	Average	0.29	0.09	0.10	0.09	0.10	0.09	0.08
	Variance	0.00	0.00	0.01	0.00	0.01	0.01	0.00
	SD	0.04	0.05	0.07	0.07	0.08	0.07	0.06
Spring	Max	0.36	0.38	0.43	0.38	0.40	0.59	0.36
	Min	0.00	0.00	0.00	0.00	0.00	0.00	0.00
	Average	0.08	0.08	0.09	0.08	0.08	0.08	0.08
	Variance	0.00	0.00	0.00	0.00	0.00	0.00	0.00
	SD	0.04	0.05	0.05	0.04	0.05	0.06	0.04
Summer	Max	0.41	0.32	0.30	0.34	0.45	0.33	0.38
	Min	0.00	0.00	0.00	0.00	0.00	0.00	0.00
	Average	0.10	0.09	0.09	0.09	0.08	0.10	0.09
	Variance	0.00	0.00	0.00	0.00	0.00	0.00	0.00
	SD	0.06	0.05	0.05	0.05	0.06	0.06	0.06
Autumn	Max	0.53	0.71	0.68	0.54	0.70	0.79	0.52
	Min	0.00	0.00	0.00	0.00	0.00	0.00	0.00
	Average	0.09	0.10	0.13	0.13	0.13	0.13	0.09
	Variance	0.00	0.01	0.01	0.01	0.01	0.01	0.01
	SD	0.07	0.07	0.10	0.09	0.11	0.11	0.07

In contrast, the western stations—Astara (10 m and 30 m)—exhibit a dominant southward flow (S, SSE), especially at the surface. At Astara (30 m), bottom currents shift toward northern and northwestern directions (NNW, NW), indicating greater directional dispersion and energy reduction with depth. Notably, at Astara (10 m), relatively fast currents from the west and southeast are evident in the speed-direction scatter diagrams, with surface currents between 0.1 and 0.2 m/s accounting for over 30%. These findings highlight the influence of coastal morphology and bathymetric variation on current behavior in the western region.

Roudsar presents a distinct exception to the general circulation pattern. At both the 10 m and 30 m stations, northern currents (NNW, N, NW) dominate in frequency, yet the faster currents are southward (SSE), as confirmed by scatter diagrams. At the 10 m station, surface currents are equally distributed between 0–0.1 m/s and 0.1–0.2 m/s, while bottom currents in the 0–0.1 m/s range comprise roughly double the percentage of those in the higher range. The 30 m station shows similar directional dominance but with greater dispersion at the bottom layer. This reversal of flow direction and velocity indicates the presence of local eddies and complex hydrodynamic interactions unique to Roudsar.

Overall, while the Caspian Sea's counterclockwise circulation governs the prevailing current directions in most stations, local factors such as depth, coastal geometry, and seasonal wind patterns introduce significant variability. The Roudsar stations, in particular, demonstrate how localized dynamics can diverge from basin-wide trends, underscoring the importance of high-resolution field measurements in coastal current analysis.

Figures 2 and 3 present the surface and bottom layer current rose, respectively. In addition, the direction distribution bar, speed distribution bar, and speed-direction scatter diagrams for three stations are presented in Figures 4 to 6 for surface layer and in Figures 7 to 9 for bottom layer, as examples.

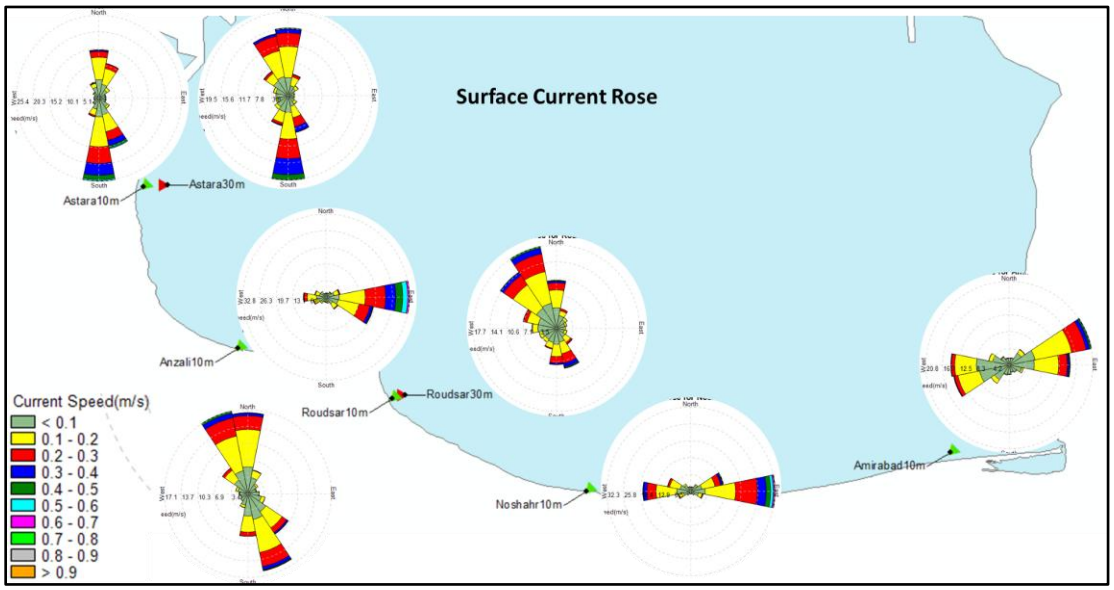

Figure. 2. Surface current roses at all measurement stations, derived from the entire observation period (December 2012–January 2014). Current velocity is shown in meters per second (m/s).

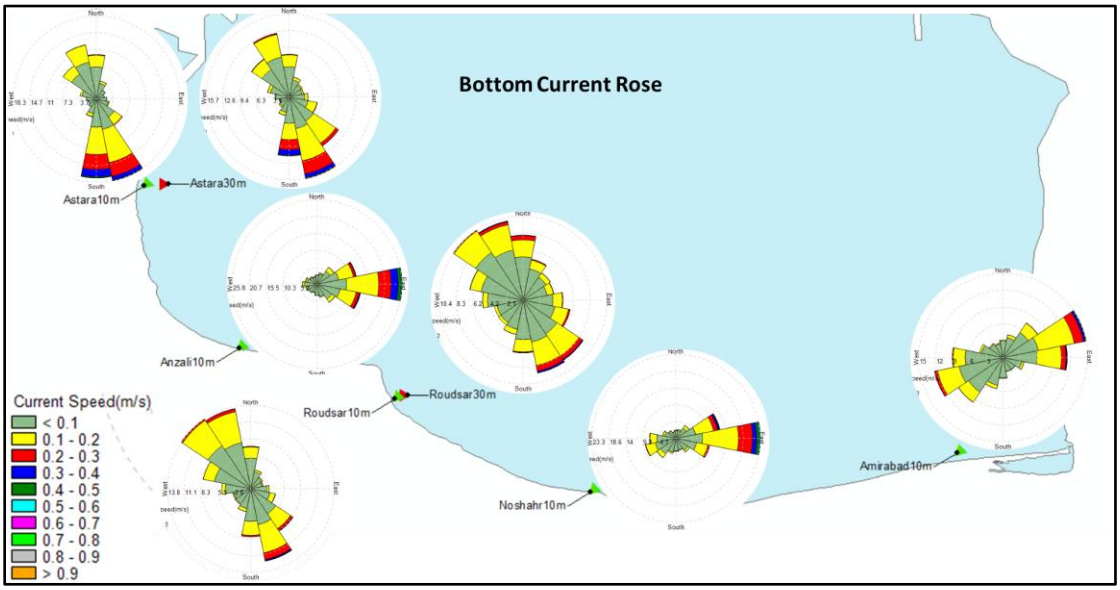

Figure. 3. Bottom current roses at all measurement stations, derived from the entire observation period (December 2012–January 2014). Current velocity is shown in meters per second (m/s).

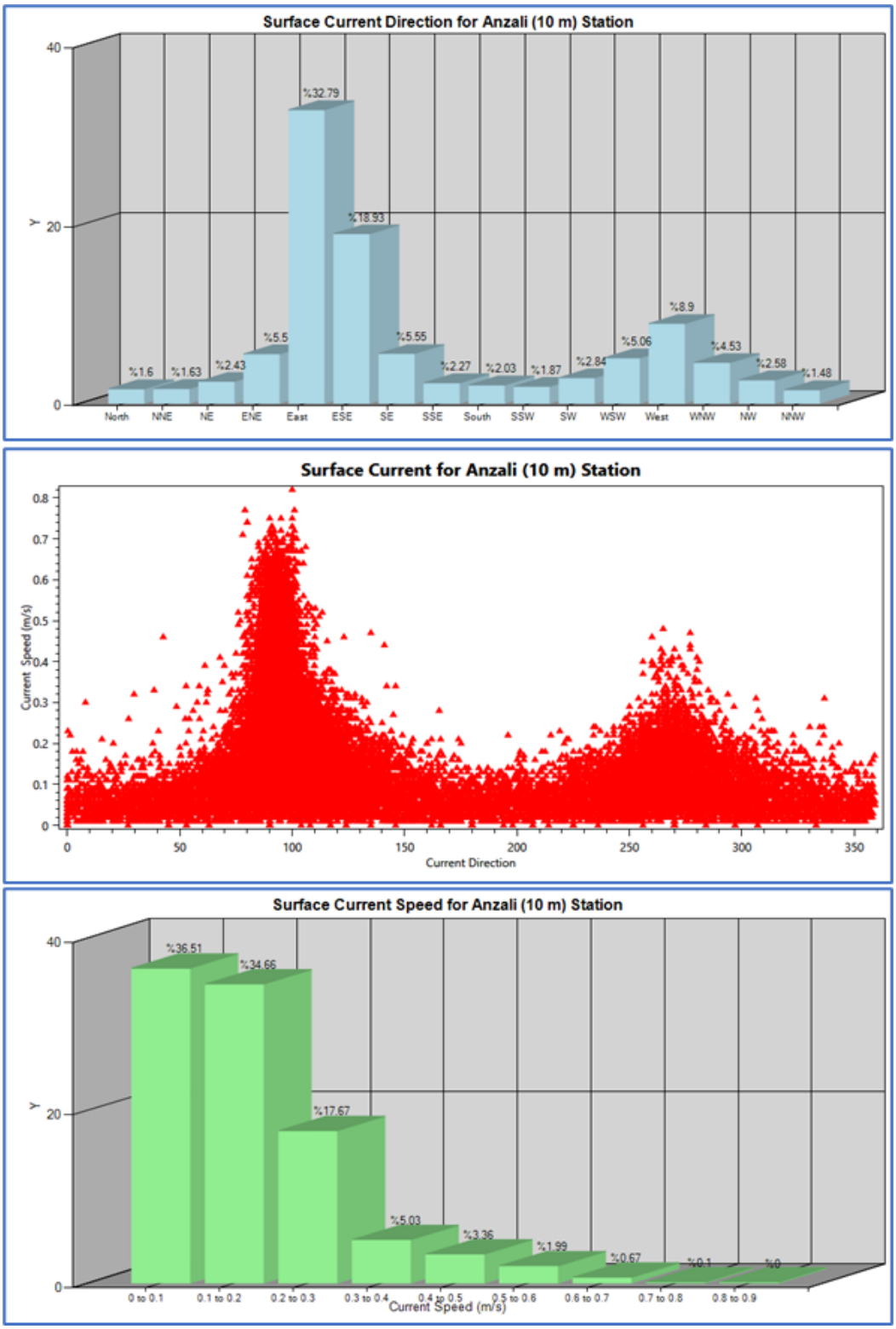

Figure. 4. Surface layer current characteristics at Anzali station (10 m depth) during the entire observation period (December 2012–January 2014). Top: direction distribution bar, and Bottom: speed distribution bar, where the Y-axis represents the percentage of occurrences. Middle: speed–direction scatter diagram. Current velocity is expressed in meters per second (m/s).

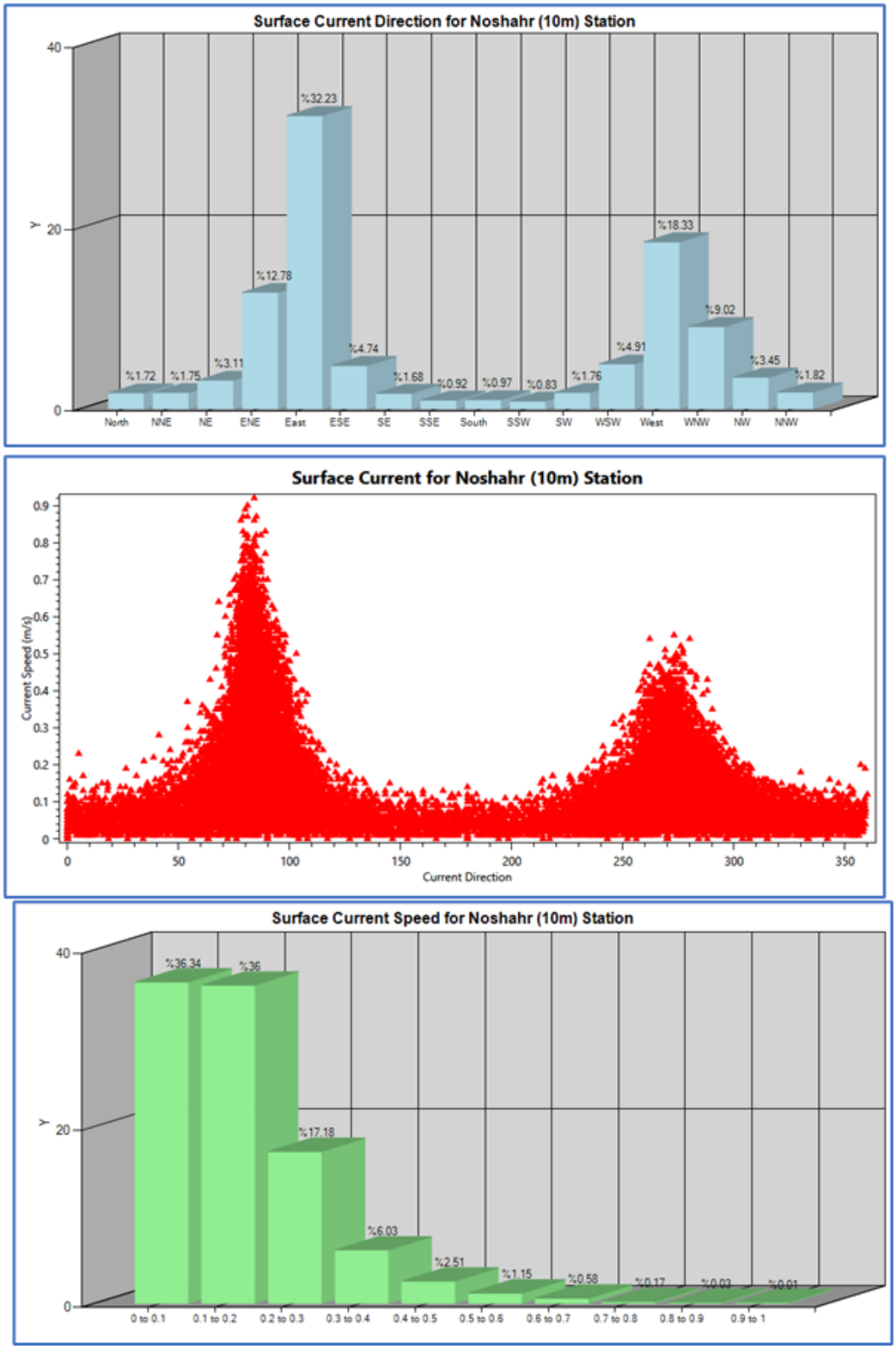

Figure. 5. Surface layer current characteristics at Noshahr station (10 m depth) during the entire observation period (December 2012–January 2014). Top: direction distribution bar, and Bottom: speed distribution bar, where the Y-axis represents the percentage of occurrences. Middle: speed–direction scatter diagram. Current velocity is expressed in meters per second (m/s).

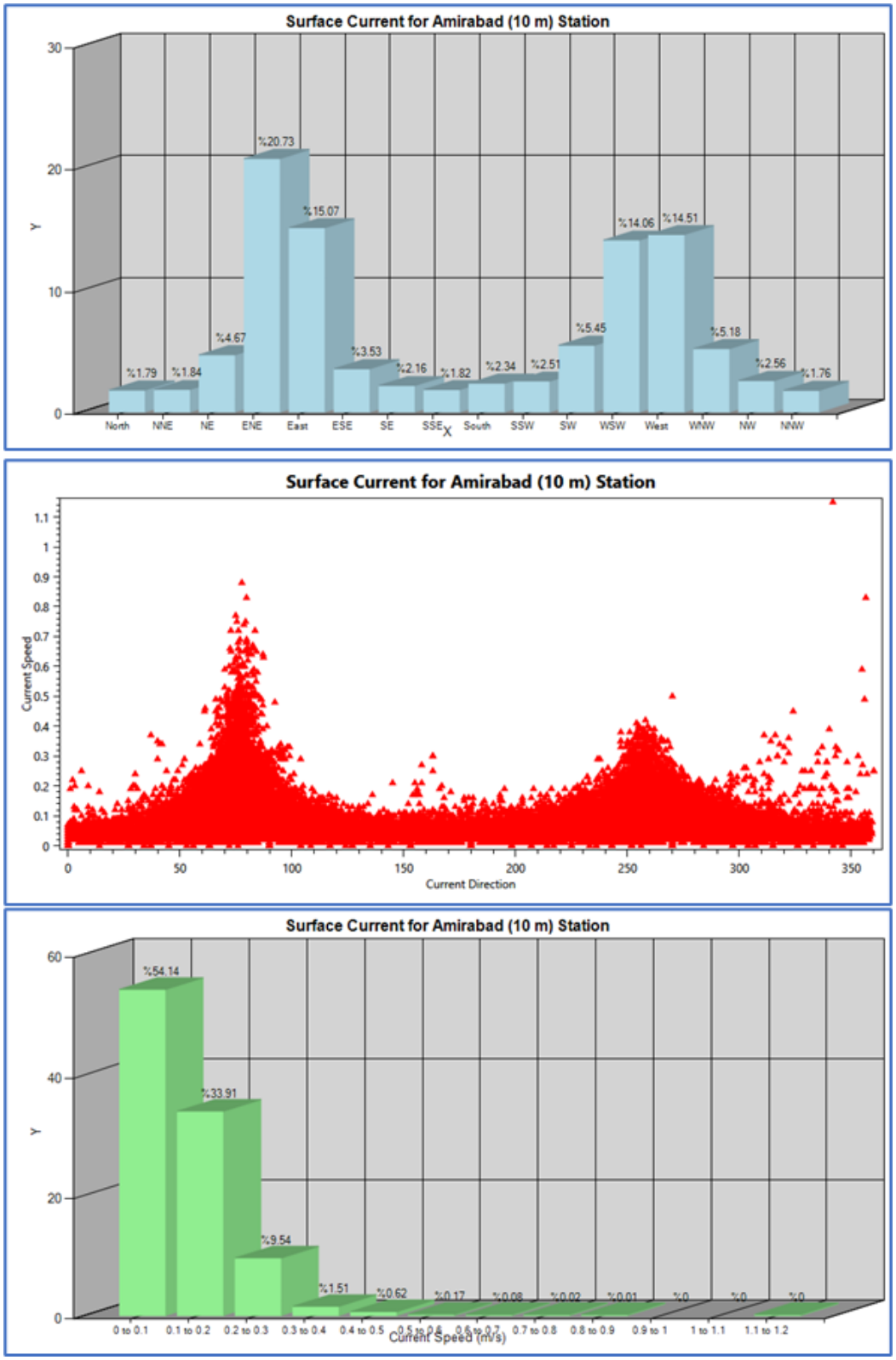

Figure. 6. Surface layer current characteristics at Amirabad station (10 m depth) during the entire observation period (December 2012–January 2014). Top: direction distribution bar, and Bottom: speed distribution bar, where the Y-axis represents the percentage of occurrences. Middle: speed–direction scatter diagram. Current velocity is expressed in meters per second (m/s).

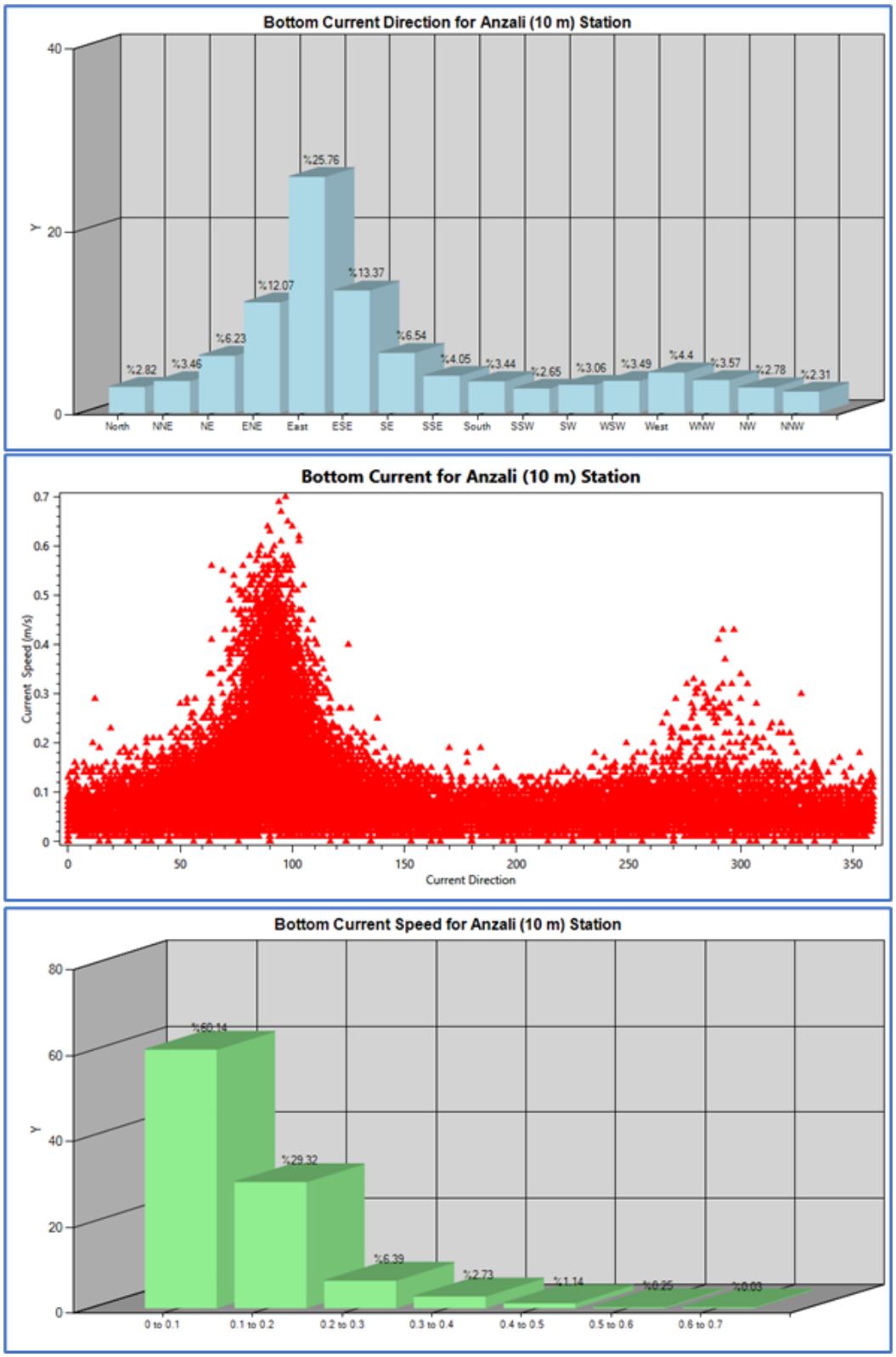

Figure. 7. Bottom layer current characteristics at Anzali station (10 m depth) during the entire observation period (December 2012–January 2014). Top: direction distribution bar, and Bottom: speed distribution bar, where the Y-axis represents the percentage of occurrences. Middle: speed–direction scatter diagram. Current velocity is expressed in meters per second (m/s).

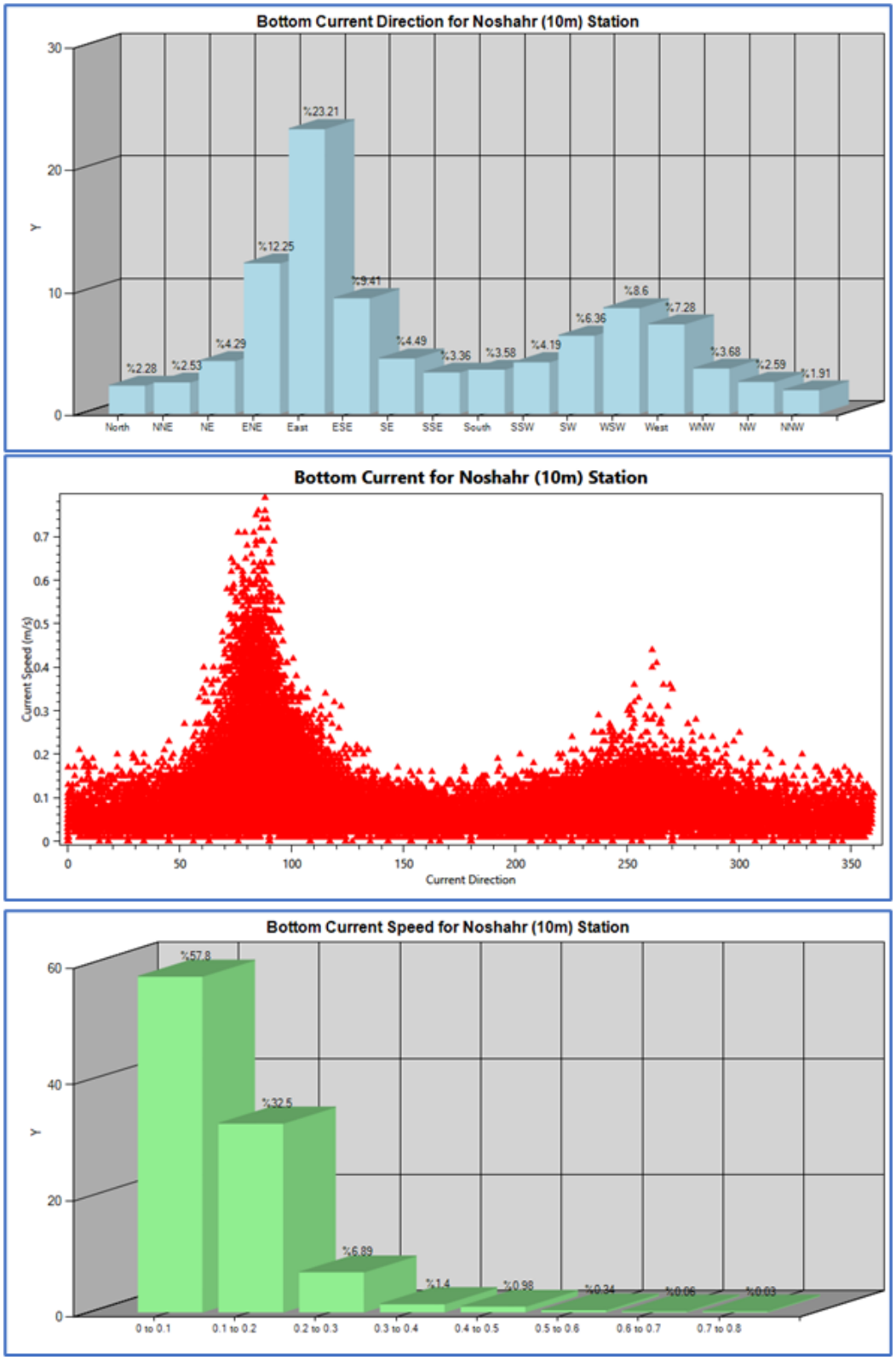

Figure. 8. Bottom layer current characteristics at Noshahr station (10 m depth) during the entire observation period (December 2012–January 2014). Top: direction distribution bar, and Bottom: speed distribution bar, where the Y-axis represents the percentage of occurrences. Middle: speed–direction scatter diagram. Current velocity is expressed in meters per second (m/s).

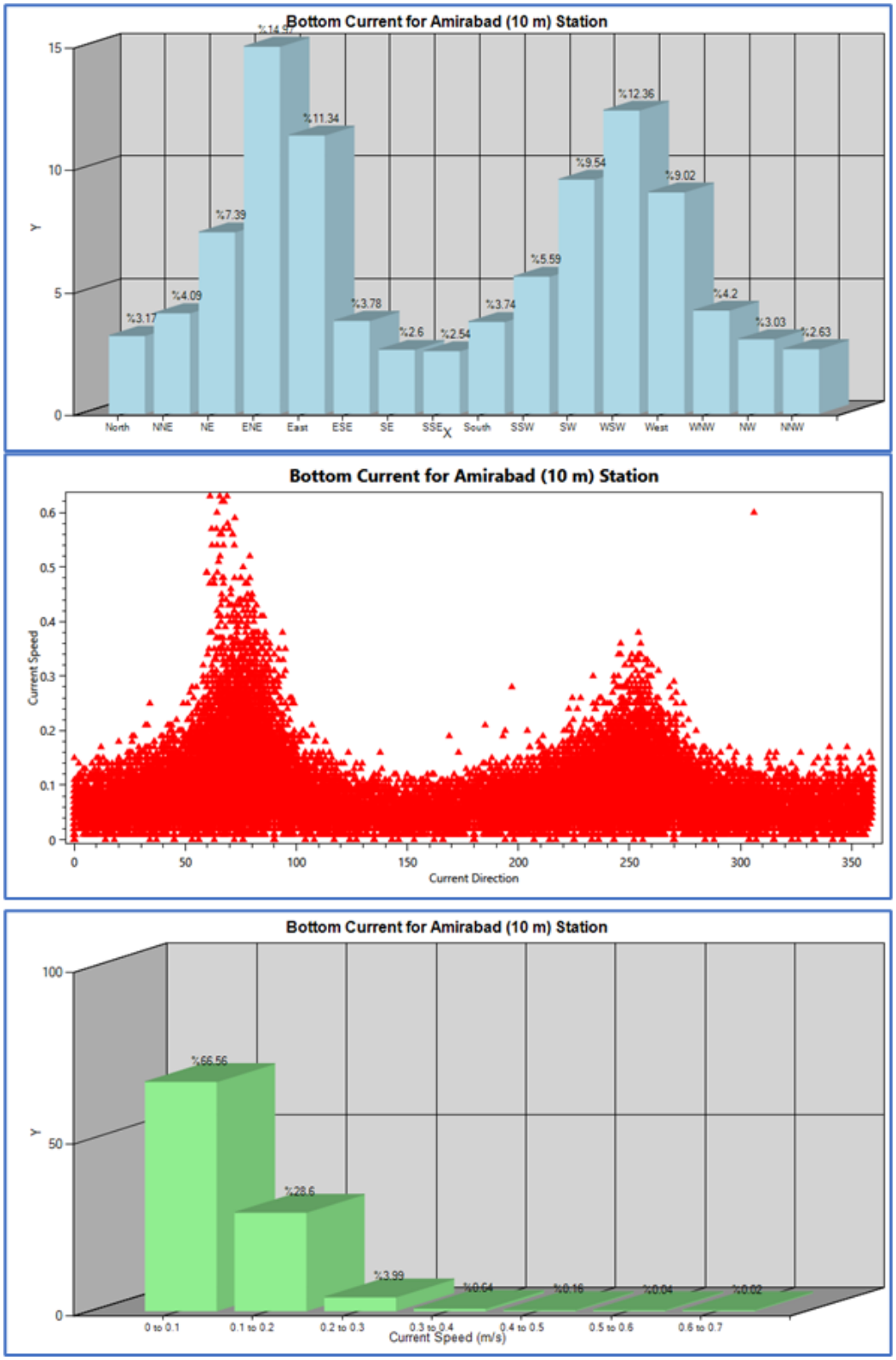

Figure. 9. Bottom layer current characteristics at Amirabad station (10 m depth) during the entire observation period (December 2012–January 2014). Top: direction distribution bar, and Bottom: speed distribution bar, where the Y-axis represents the percentage of occurrences. Middle: speed–direction scatter diagram. Current velocity is expressed in meters per second (m/s).

Seasonal analysis of current directions across the southern Caspian Sea stations reveals distinct regional patterns influenced by depth and coastal morphology. In central and eastern stations such as Noshahr, Anzali, and Amirabad (all at 10 m depth), the prevailing current direction at both surface and seabed is consistently eastward (E, ENE, ESE), with the highest frequency occurring in winter. For example, at Noshahr, the surface currents are dominantly E, followed by W and ENE, all peaking in winter. Similarly, Anzali shows a strong eastward flow (E, ESE) in both layers during winter, with weaker westward currents (W, ENE) appearing in autumn. At Amirabad, the prevailing currents (ENE, E) are most frequent in summer, while the tertiary direction (W) peaks in winter. These observations suggest that winter winds intensify eastward currents in most stations, while summer introduces localized shifts, particularly in Amirabad.

Western stations such as Astara exhibit a contrasting pattern. At both 10 m and 30 m depths, the prevailing current direction is southward (S, SSE), with the highest frequency in winter. However, spring introduces notable reversals: at the surface, northern currents (N, NNW) become more frequent, while at the seabed, NNW and NW directions dominate. This seasonal shift indicates the influence of wind-driven circulation and bathymetric modulation, especially in deeper layers. The Astara (10 m) station shows a similar trend, with S and SSE currents prevailing in winter and northern flows (N, NNW) gaining prominence in spring.

Roudsar stations present a unique seasonal behavior. At the 10 m station, surface currents are predominantly NNW throughout the year, peaking in spring, while SSE currents—though less frequent—also reach their maximum in spring. At the seabed, NW and NNW currents dominate in winter, with SSE currents maintaining a consistent presence. The 30 m station follows a similar pattern: surface currents (N, NW, NNW) peak in spring, while bottom currents (NNW, NW) are most frequent in winter. The near-equal seasonal distribution of other directions in the bottom layer suggests a complex and balanced current regime influenced by local eddies and topographic features.

In summary, while winter generally intensifies eastward and southward currents across most stations, spring introduces directional reversals, particularly in Roudsar and Astara. These seasonal shifts underscore the dynamic interplay between regional wind systems and coastal morphology in shaping current patterns along the southern Caspian Sea.

Figures 10 and 11 present a radar chart of the seasonal current direction of the surface and bottom layer.

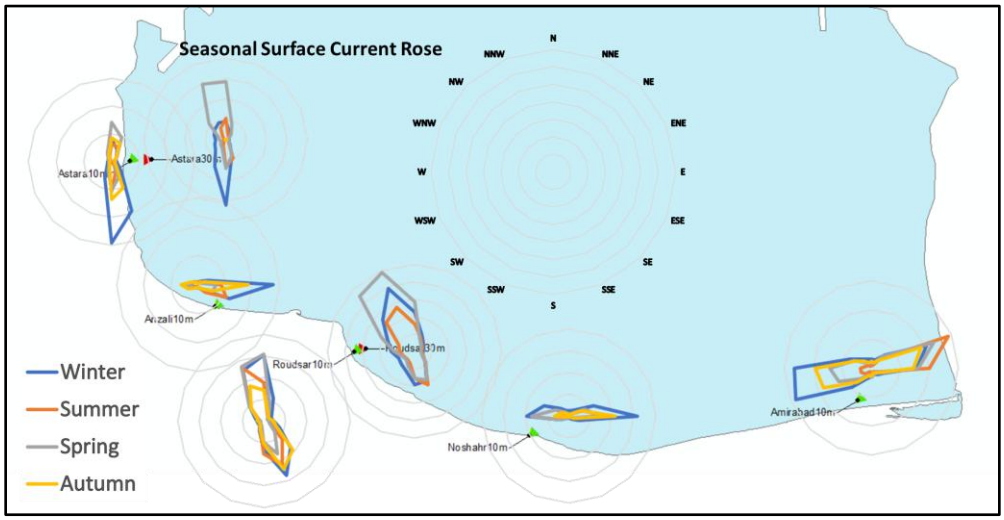

Figure. 10. Radar chart of seasonal current direction in the surface layer at all measurement stations, showing variations across Winter, Spring, Summer, and Autumn during the observation period (December 2012–January 2014).

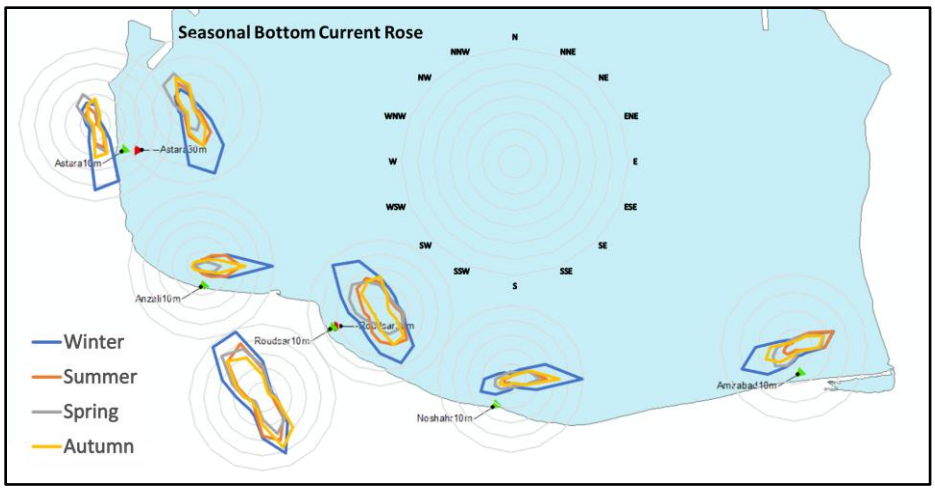

Figure. 11. Radar chart of seasonal current direction in the Bottom layer at all measurement stations, showing variations across Winter, Spring, Summer, and Autumn during the observation period (December 2012–January 2014).

3-2. Wave

This section presents the descriptive statistical indicators of significant wave height recorded across seven coastal stations over four seasons. The parameters analyzed include mean, maximum, minimum, variance, and standard deviation, allowing for both seasonal and spatial comparisons of wave behavior. Overall, autumn exhibited the highest variability in wave conditions across the stations. In this season, variance values exceeded 0.6 at several locations, with standard deviations reaching up to 0.83 meters. These elevated values reflect a wide dispersion in wave height data, indicating the presence of highly variable wave events. Such fluctuations are likely driven by a combination of strong wind activity, atmospheric pressure changes, and unstable sea surface conditions. In contrast, spring recorded the lowest wave variability, with variance values generally below 0.15 and standard deviations under 0.35 meters, suggesting relatively stable wave regimes during this period. In terms of seasonal averages, the mean significant wave height in winter ranged from 0.5 to 0.72 meters across most stations, accompanied by relatively high standard deviations (up to 0.64 meters). This concurrence of elevated mean and dispersion values points to turbulent and unstable wave conditions during the colder months. During summer, mean wave heights ranged between 0.34 and 0.79 meters, yet standard deviations remained high at certain stations (up to 0.42 meters), indicating the coexistence of calm intervals with sporadic high-energy wave events. Across all stations, the highest annual variance was recorded at 0.69, with a corresponding maximum standard deviation of 0.83 meters—both indicative of pronounced wave instability and variability. Conversely, the lowest recorded variance was 0.04, and the minimum standard deviation was 0.20 meters, reflecting more uniform and consistent wave conditions. These statistical contrasts highlight that while some coastal zones are subject to intense wave fluctuations, others maintain relatively stable hydrodynamic profiles. In summary, the analysis of variance and standard deviation reveals that wave dynamics along the southern Caspian Sea coast are both seasonally and spatially heterogeneous. In particular, autumn and winter are characterized by elevated wave dispersion, which may significantly influence sediment transport processes, shoreline erosion patterns, and the design criteria for coastal infrastructure. A detailed summary of the descriptive statistics for significant wave height across all stations is presented in Table 4. Having outlined the statistical characteristics of wave height, the next section focuses on interpreting wave direction and energy patterns in a spatial and temporal context. Wave direction and energy patterns along the southern Caspian Sea coast exhibit distinct regional and seasonal characteristics. In most stations, waves predominantly originate from northern sectors, with variations in direction and height influenced by local morphology and seasonal wind regimes.

Table 4. Descriptive Statistics of Significant Wave Height at Seven Coastal Stations Across Four Seasons

		Roudsar 30m	Roudsar 10m	Astara 10m	Astara 30m	Anzali 10m	Noshahr 10m	Amirabad 10m
Winter	Max	3.1	2.3	1.75	3.83	3.5	3.37	4.72
	Min	0.02	0.08	0.07	0.02	0.13	0.04	0.02
	Average	0.72	0.56	0.53	0.66	0.69	0.65	0.5
	Variance	0.3	0.15	0.1	0.23	0.41	0.28	0.18
	SD	0.55	0.39	0.32	0.48	0.64	0.52	0.43
Spring	Max	2.12	1.59	1.53	2.63	2.8	2.46	2.54
	Min	0.03	0.03	0.03	0.06	0.13	0.03	0.04
	Average	0.46	0.4	0.37	0.56	0.53	0.55	0.51
	Variance	0.11	0.07	0.06	0.09	0.2	0.13	0.08
	SD	0.33	0.26	0.24	0.3	0.44	0.36	0.29
Summer	Max	1.96	3.48	1.16	1.38	2.82	2.31	2.66
	Min	0.09	0.08	0.6	0.01	0.02	0.14	0.02
	Average	0.54	0.45	0.34	0.45	0.79	0.66	0.66
	Variance	0.13	0.07	0.04	0.06	0.13	0.17	0.1
	SD	0.36	0.27	0.2	0.25	0.37	0.42	0.32
Autumn	Max	3.73	3.28	2.64	3.62	4.47	3.73	2.39
	Min	0	0.02	0.08	0.11	0.12	0.09	0.01
	Average	0.74	0.62	0.61	0.81	0.99	0.74	0.55
	Variance	0.32	0.24	0.16	0.33	0.69	0.41	0.2
	SD	0.56	0.49	0.4	0.57	0.83	0.64	0.45

At central stations such as Noshahr and Anzali (both 10 m depth), the prevailing wave direction is N (30%), followed by NNW or NNE (26%). In Noshahr, waves from N typically exhibit significant wave heights between 0.0 and 0.4 m or 0.4 and 0.8 m, while other directions are dominated by lower-energy waves. Seasonal analysis shows that N waves are most frequent in winter, autumn, and spring, whereas NNW waves peak in summer. Anzali displays a similar pattern, with N and NNE waves dominating across seasons. Notably, Anzali records the highest energy levels among all stations, with frequent waves reaching 0.8 to 1.2 m in height. These findings highlight the energetic nature of the central coast, especially during colder months.

In the easternmost station, Amirabad (10 m), the prevailing wave direction shifts westward, with NW waves accounting for 36% and NNW for 28% of occurrences. The most frequent waves have significant wave heights between 0.0 and 0.8 m. Seasonally, NW and NNW waves dominate in winter and spring, while NW waves remain prevalent in summer and autumn. This pattern suggests a localized influence of wind and coastal orientation on wave generation in the eastern sector.

Western stations such as Astara show a strong dominance of northeastward waves. At Astara (30 m), NE waves constitute 35% of total occurrences, with significant wave heights between 0.4 and 0.8 m. These waves are most frequent in summer, autumn, and winter, while ESE waves dominate in spring. The shallower Astara (10 m) station reinforces this trend, with NE waves comprising 40% and ENE waves 23% of the total. In this station, NE waves span both low and moderate energy ranges (0.0–0.8 m), while other directions are generally associated with lower wave heights. The seasonal distribution confirms the dominance of NE waves in most seasons, with spring introducing a shift toward ESE.

Roudsar stations present a transitional pattern between central and western regimes. At the 10 m station, over 60% of waves originate from NNE

(32%) and NE (29%), with significant wave heights ranging from 0.0 to 0.8 m. NNE waves are most frequent in summer and autumn, while NE waves prevail in winter. The deeper Roudsar (30 m) station shows a similar distribution, with NNE (26%) and N (25%) waves accounting for over half of the total. These waves typically fall within the 0.4–0.8 m range. Seasonal variation is subtle, with N waves dominating in summer and spring, and NNE waves in autumn and winter. The close frequency between these directions across seasons suggests a stable wave regime influenced by consistent wind forcing.

In summary, while northern and northeastern wave directions dominate across most stations, regional differences in wave height and seasonal frequency reflect the interplay between local coastal geometry and atmospheric conditions. Anzali and Astara stand out as high-energy zones, whereas Roudsar and Amirabad exhibit transitional and localized wave behaviors.

Figure 12 shows a significant wave rose for all stations. In Figure 13, Radar charts of the seasonal wave direction are presented. In addition, Figure 14 presents significant wave probability for three stations.

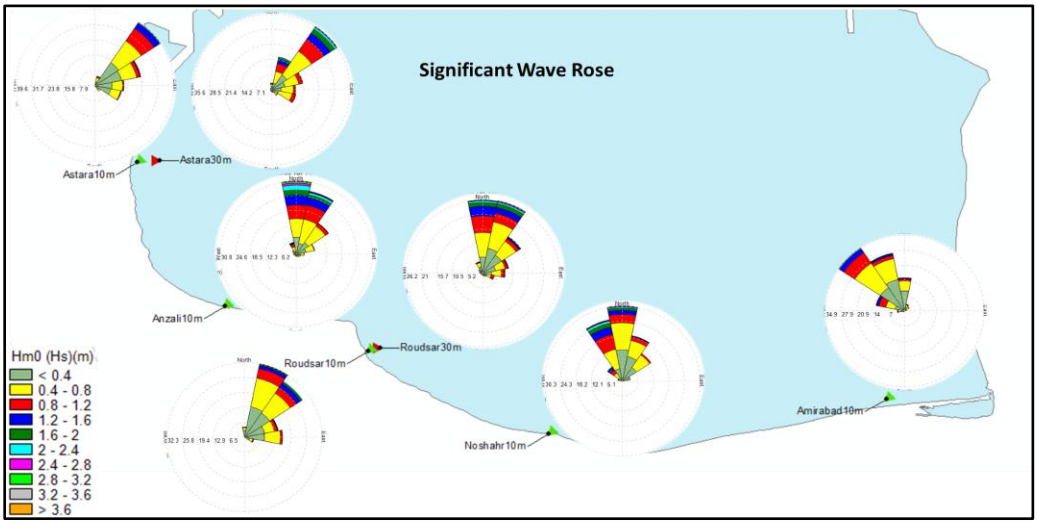

Figure. 12. Significant wave roses for all measurement stations, derived from the entire observation period (December 2012–January 2014). Wave height is expressed in meters (m)

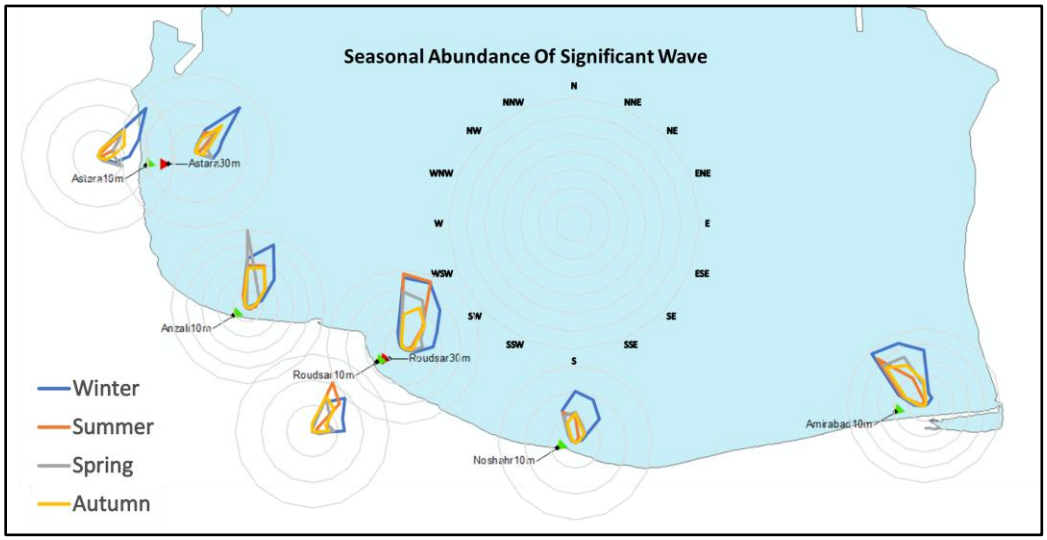

Figure. 13. Radar charts of seasonal wave direction at all measurement stations, showing variations across Winter, Spring, Summer, and Autumn during the observation period (December 2012–January 2014).

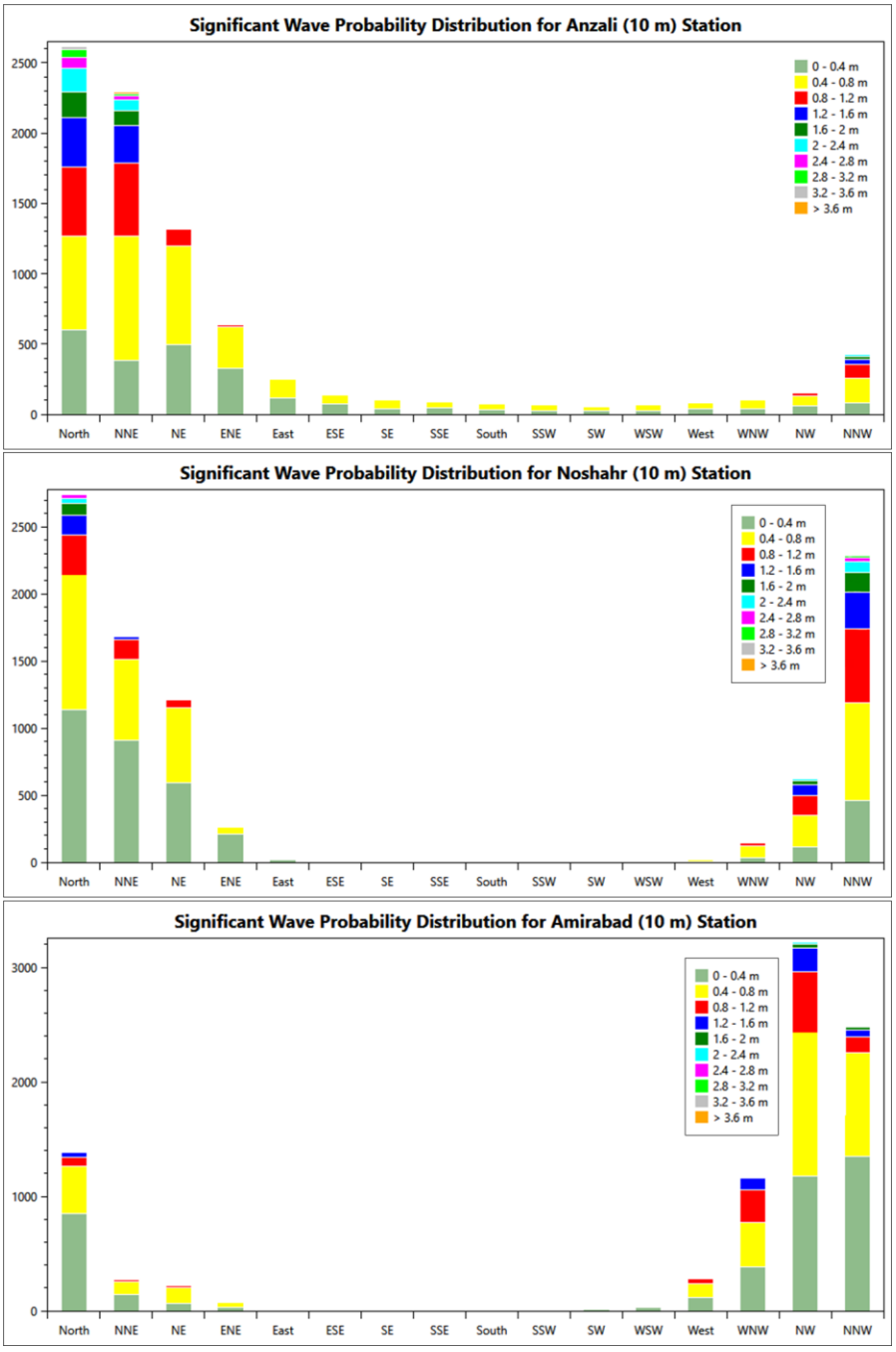

Figure. 14. Probability distributions of significant wave height at Anzali (top), Noshahr (middle), and Amirabad (bottom) stations, derived from the entire observation period (December 2012–January 2014).

4. Discussion

This section discusses the spatial and temporal patterns of currents and waves across the measuring stations. It compares prevailing and reversing currents in surface and bottom layers across seasons and examines differences in directional extent and energy levels between stations. The results highlight the complexity of current dynamics and the influence of seasonal and geographical factors on hydrodynamic behavior along the southern Caspian Sea coast.

4-1. Currents

At Roudsar (10 m), prevailing currents in both layers originate from the NNW direction. Although SSE currents are less frequent, they

exhibit higher velocities, indicating dynamic variability. The frequency distribution shows minimal differences between NNW and SSE flows, and the dominance of low-speed currents (0–0.2 m/s) suggests a low-energy regime. At Roudsar (30 m), similar NW to NNW currents are observed, but with greater directional variability and a more balanced distribution of prevailing and reversing flows, especially in the bottom layer. Seasonally, surface currents peak in spring, while bottom currents are most frequent in winter. At Noshahr (10 m), a prevailing eastward current dominates both layers. The bottom layer shows slower and more variable currents, suggesting stratification and reduced energy with depth. Eastward currents are most frequent in winter.

At both Astara stations, prevailing currents originate from the south, with notable differences between the 10 m and 30 m stations. Reversing currents are weaker at the 10 m station, especially at the surface, indicating atmospheric influence. Bottom currents are slower and more variable, again suggesting energy reduction with depth. Currents from N and NNW are most frequent in spring, while S and SSE currents dominate in winter. At Anzali (10 m), prevailing eastward currents are significantly more frequent than reversing westward flows. ENE currents are weaker at the surface than at depth, likely due to wind and wave influence. Eastward currents peak in winter across both layers. At Amirabad (10 m), prevailing ENE currents are accompanied by frequent reversing WSW flows, especially in winter. The prevailing current maintains relatively equal frequency across other seasons, observed in both layers. This pattern is likely influenced by dominant northeast winds that oppose the Caspian Sea's counterclockwise circulation (Figure 15), reinforcing localized reverse flows.

4-2. Wave

Significant wave height conditions are relatively similar across stations. At 30 m depth stations (Roudsar, Astara, and Anzali), most frequent waves range from 0.4 to 0.8 m. At other stations, wave heights range from 0.0 to 0.8 m. Anzali (10 m) stands out with frequent waves between 0.8 and 1.2 m, indicating it as the most energetic station in terms of wave height. Prevailing wave directions at western stations are between N and NE, while eastern stations show directions between N and NW. At Noshahr (10 m), the dominant wave direction is N. Waves are most frequent in winter across stations, except at Anzali (10 m), where spring slightly exceeds winter. At Roudsar stations, summer and winter frequencies are nearly equal. Seasonal variations are evident. At Anzali (10 m), NNE waves dominate in winter, summer, and autumn, while N waves prevail in spring. At Roudsar (10 m), NNE waves dominate in summer and autumn, and NE waves in winter, reflecting strong seasonal influence on wave patterns.

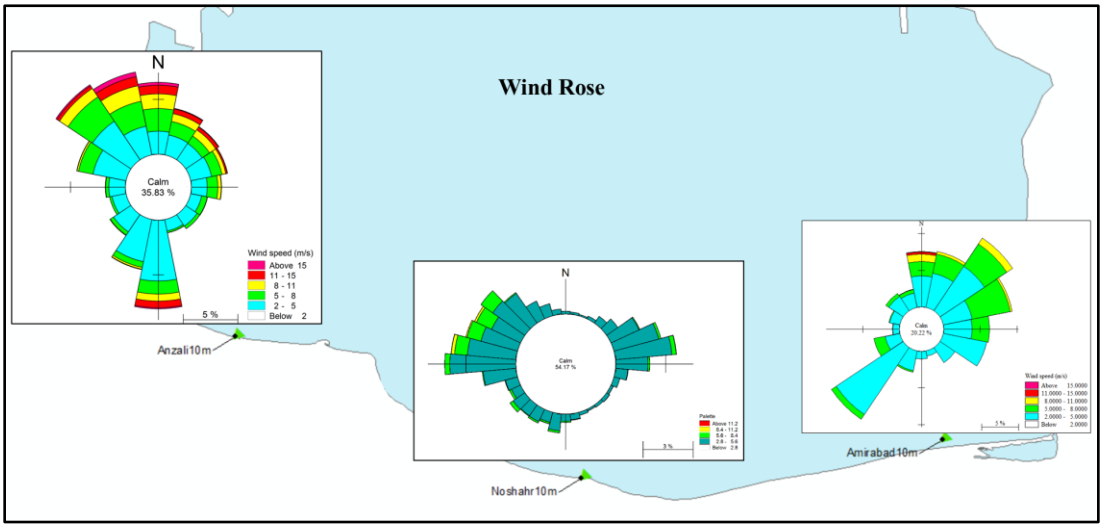

Figure. 15. Wind rose diagrams at Anzali, Noshahr, and Amirabad stations, recorded simultaneously with ADCP measurements during the observation period (December 2012–January 2014). Data derived from coastal meteorological records.

5. Conclusion

Given the purposeful selection of stations based on coastal and marine engineering considerations, this section summarizes the spatial and temporal patterns of waves and currents across the study area, including comparisons of dominant and reversing currents in surface and bottom layers across seasons.

The findings confirm the overall counterclockwise circulation of currents in the Caspian Sea, evident in prevailing directions at most stations. Along the northern coasts (Astara), currents are southward, while eastern coasts (Anzali, Noshahr, Amirabad) show eastward flows (Firoozfar et al., 2014; Ghaffari & Chegini, 2010; Ibrayev et al., 2010). These directions generally align with coastal morphology (Firoozfar et al., 2014). Offshore stations exhibit greater directional variability, emphasizing the role of shoreline configuration. The combined influence of wind, waves, and morphology is particularly evident at Amirabad and Anzali (Dodet et al., 2019; Johansson et al., 2022; Melet et al., 2020).

While Zavialov et al. (2024) emphasized basin-scale circulation using satellite altimetry, the present study complements their findings by offering finer spatial resolution and site-specific current responses based on in-situ measurements. At Amirabad (10 m), wind and wave setup contribute to water accumulation along the southeastern coast, intensifying alongshore currents and enhancing reversing W and WSW flows. A similar effect at Anzali (10 m) amplifies eastward currents while weakening westward reversals. These observations underscore the impact of wind and wave conditions on current behavior. At Roudsar stations, current dynamics deviate from the general circulation, likely due to cyclonic activity and coastal orientation changes (Bakhtiari et al., 2024). Prevailing currents and waves are most frequent in winter across stations. Seasonal variation in current and wave directions further highlights the temporal complexity of hydrodynamic regimes. The spatially resolved data presented here provide a valuable baseline for future modeling efforts. In particular, the observed patterns may inform numerical models such as SWAN (for wave propagation) and ROMS (for hydrodynamic circulation), enabling scenario-based projections under climate change. Recent CMIP6-based projections suggest that reduced river inflow and increased evaporation may lead to substantial Caspian Sea level decline by the end of the 21st century (Samant & Prange, 2023).

Under high-emission scenarios such as SSP5-8.5, projected shifts in wind regimes and declining sea levels may significantly alter nearshore circulation patterns, particularly in semi-enclosed regions like Amirabad.

Future studies should integrate these models with regional climate projections to assess potential impacts on sediment transport, shoreline stability, and coastal infrastructure planning.

Despite the valuable insights provided, this study is subject to several limitations that should be considered when interpreting the results. Measurements were restricted to coastal stations, which means that the findings primarily reflect nearshore conditions and cannot be generalized to the entire Caspian basin. The dataset covers only a single annual cycle, limiting the ability to capture interannual or long-term variability. A small portion of the data was lost or excluded during the recording and quality control processes, which may have slightly reduced the completeness of the dataset. Furthermore, the number of stations was limited and confined to the southern sector of the Caspian Sea, thereby reducing the spatial representativeness of the results. Acknowledging these limitations highlights the need for future research with broader spatial coverage, extended temporal monitoring, and more comprehensive datasets to achieve a deeper understanding of hydrodynamic processes in the region.

Acknowledgment

The Iranian Port and Maritime Organization (PMO) supported this research and retains all financial and intellectual property rights related to it. The Laboratory and Research Center of the Ministry of Energy, Pouya Tarh Pars, and Namrood Consulting Company in Iran also participated in this research. We hereby thank them.

Author Contributions:

Abbas Einali: Statistical analysis, visualization, data interpretation, and writing – original draft preparation.

Mohammad Akbari Nasab: Data analysis and interpretation.
Mohammad Hossein Nemati: Data acquisition and field measurement operations.

Conflicts of interest

The authors of this article declared no conflict of interest regarding the authorship or publication of this article.

Data availability statement:

All data generated or analyzed during this study are included in this published article.

References

Alemi Safaval, P., Kheirkhah Zarkesh, M., Neshaei, S., & Ejlali, F. (2018). Morphological changes in the southern coasts of the Caspian Sea using remote sensing and GIS. Caspian Journal of Environmental Sciences, 16(3), 271-285. doi: 10.22124/cjes.2018.3067

Azizpour, J., & Ghaffari, P. (2023). Low-frequency sea level changes in the Caspian Sea: long-term and seasonal trends. Climate Dynamics, 61(5), 2753-2763. doi: 10.1007/s00382-023-06715-9

Bakhtiari, A., Shad, E., & Siadatmousavi, S. M. (2024). Exploring submesoscale eddies in the southern Caspian sea: A focus on rudsar and Sefidrud regions. Deep Sea Research Part I: Oceanographic Research Papers, 208, 104316. doi: 10.1016/j.dsr.2024.104316

Bellafiore, D., Bucchignani, E., Gualdi, S., Carniel, S., Djurdjeviæ, V., & Umgiesser, G. (2011). Evaluating meteorological climate model inputs to improve coastal hydrodynamic studies. Advances in Science and Research, 6(1), 227-231. doi: 10.5194/asr-6-227-2011

Birch, R., Fissel, D. B., Borg, K., Lee, V., & English, D. (2004). The capabilities of Doppler current profilers for directional wave measurements in coastal and nearshore waters Oceans' 04 MTS/IEEE Techno-Ocean'04 (IEEE Cat. No. 04CH37600), https://ieeexplore.ieee.org/document/1406330

Chicherina, O., Leonov, A., & Fashchuk, D. Y. (2004). Geographical and ecological characteristics of the caspian sea and modern tendencies in the evolution of its ecosystem. Water Resources, 31, 271-289. doi: 10.1023/b:ware.0000028697.51386.aa

Dodet, G., Melet, A., Ardhuin, F., Bertin, X., Idier, D., & Almar, R. (2019). The contribution of wind-generated waves to coastal sea-level changes. Surveys in Geophysics, 40(6), 1563-1601. doi: 10.1007/s10712-019-09557-5

Firoozfar, A., Neshaei, M. A. L., & Dykes, A. P. (2014). Beach profiles and sediments, a case of Caspian Sea. International Journal of Marine Science, 4(43). https://www.aquapublisher.com/index.php/ijms/article/html/1316/

Ghaffari, P., & Chegini, V. (2010). Acoustic Doppler Current Profiler observations in the southern Caspian Sea: shelf currents and flow field off Feridoonkenar Bay, Iran. Ocean Science, 6(3), 737-748. doi: 10.5194/os-6-737-2010

Gould, J., Sloyan, B., & Visbeck, M. (2013). In situ ocean observations: A brief history, present status, and future directions. International Geophysics, 103, 59-81. doi: 10.1016/B978-0-12-391851-2.00003-9

Ibrayev, R., Özsoy, E., Schrum, C., & Sur, H. (2010). Seasonal variability of the Caspian Sea three-dimensional circulation, sea level and air-sea interaction. Ocean Science, 6(1), 311-329. doi: 10.5194/os-6-311-2010

Johansson, M. M., Björkqvist, J.-V., Särkkä, J., Leijala, U., & Kahma, K. K. (2022). Correlation of wind waves and sea level variations on the coast of the seasonally ice-covered Gulf of Finland. Natural Hazards and Earth System Sciences, 22(3), 813-829. doi: 10.5194/nhess-22-813-2022

Lavrova, O. Y., Mityagina, M., Sabinin, K., & Serebryany, A. (2011). Satellite observations of surface manifestations of internal waves in the Caspian Sea. Izvestiya, Atmospheric and Oceanic Physics, 47, 1119-1126. doi: 10.1134/s000143381109009x

Mamaev, V. (2002). Europe's biodiversity–biogeographical regions and seas. Seas around Europe. The Caspian Sea–enclosed and with many endemic species. In European Environment Agency. https://www.eea.europa.eu/en/analysis/publications/report_2002_0524_154909

Masoud, M., Pawlowicz, R., & Namin, M. M. (2019). Low frequency variations in currents

on the southern continental shelf of the Caspian Sea. Dynamics of Atmospheres and Oceans, 87, 101095. doi: 10.1016/j.dynatmoce.2019.05.004

Melet, A., Almar, R., Hemer, M., Le Cozannet, G., Meyssignac, B., & Ruggiero, P. (2020). Contribution of wave setup to projected coastal sea level changes. Journal of Geophysical Research: Oceans, 125(8), e2020JC016078. doi: 10.1029/2020jc016078

Nejat, S., Hermidas Bavand, D., & Farshchi, P. (2018). Environmental challenges in the Caspian Sea and international responsibility of its littoral states. Caspian Journal of Environmental Sciences, 16(2), 97-110. doi: 10.22124/cjes.2018.2953

Nortek. (2025a). Aquadopp (Acoustic wave and current Profiler). Nortek. Retrieved 04/01/2025 from https://www.nortekgroup.com/products/aquadopp-profiler2-1-mhz

Nortek. (2025b). AWAC (Acoustic wave and current Profiler). Nortek. Retrieved 04/01/2025 from https://www.nortekgroup.com/products/awac2-1-mhz

PMDynamics_Team. (2018). PMDynamics User Guide. Ports and Maritime Organization of Iran. https://pmodynamics.pmo.ir/

Rao, L., Wang, C., Deng, K., Zhang, Z., & Lu, S. (2017). Surface wave measurement with ADCP: A review of publications from 1979 to 2017. OCEANS 2017-Anchorage, 1-7. https://ieeexplore.ieee.org/abstract/document/8232101/references#references

Samant, R., & Prange, M. (2023). Climate-driven 21st century Caspian Sea level decline estimated from CMIP6 projections. Commun Earth Environ 4, 357, 2023. doi: 10.1038/s43247-023-01017-8

Thomas, A., & Cheung, W. W. L. (2024). Impacts of Climate Change. Frontiers for Young Minds. doi: 10.3389/frym.2024.1355408

Williams, A. J. (1996). Current measurement technology development progress in the'90s-a review OCEANS 96 MTS/IEEE Conference Proceedings. The Coastal Ocean-Prospects for the 21st Century, doi: 10.1109/oceans.1996.572555

Williams, A. J. (2011). Innovative technology in oceanography: Past, present and future 2011 International Symposium on Ocean Electronics, doi: 10.1109/sympol.2011.6170491

Zavialov, P. O., Kostianoy, A. G., Sapozhnikov, P. V., Khan, V. M., Kurbaniyazov, N. K., & Kurbaniyazov, A. K. (2024). First long-term measurements on Kazakhstan shelf of the Caspian Sea reveal alternating currents and energetic temperature variability. Journal of Marine Science and Engineering, 12(11), 1957. doi: 10.3390/jmse12111957